minerals

MDPI

Article

Nature and Evolution of Paleoproterozoic Sn and Rare Metal Albitites from Central Brazil: Constraints Based on Textural, Geochemical, Ar-Ar, and Oxygen Isotopes

Ana Rita F. Sirqueira [1], Márcia A. Moura [1,*], Nilson F. Botelho [1] and T. Kurt Kyser [2,†]

[1] Instituto de Geociências, Universidade de Brasília, Campus Darcy Ribeiro, Brasília 70910-900, Brazil; ana_rita_felix@hotmail.com (A.R.F.S.); nilsonfb@unb.br (N.F.B.)

[2] Department of Geological Sciences and Geological Engineering, Queen's University, 36 Union Street, Kingston, ON K7L 3N6, Canada; kyser@geol.queensu.ca

* Correspondence: mamoura@unb.br

† Professor T. Kurt Kyser, Fellow of the Royal Society of Canada and pioneering geochemist, died while teaching in Bermuda on 29 August 2017.

Received: 30 June 2018; Accepted: 3 August 2018; Published: 8 September 2018

Abstract: Economic and subeconomic concentrations of Sn, In, rare earth elements (REE), Ta, and Nb are known in Central Brazil, in the Goias Tin Province. The Sn-P enriched albitites studied in this paper occur in sharp contact with peraluminous granites of the Aurumina Suite (2.0–2.17 Ga) and schists of the Archean to Paleoproterozoic Ticunzal Formation, as dikes or lenses from late-stage magma of the peraluminous magmatism, probably in granite cupolas. Geological, petrological, and isotopic studies were conducted. The albitites consist of albite, quartz, cassiterite, apatite, K-feldspar, and muscovite, and have magmatic texture, such as alignment of albite laths, and snowball texture in quartz, apatite, and cassiterite. They are enriched in Na_2O, P_2O_5, Sn, Ta, and Nb (Ta > Nb), and depleted in CaO, K_2O, TiO_2, MgO, Sr, Ba, Th, and REE. $^{40}Ar/^{39}Ar$ in muscovite gave a plateau age of 1996.55 ± 13 Ma, interpreted as approaching the crystallization age. Oxygen isotope data in albite-cassiterite pairs resulted in an equilibrium temperature of 653–1016 °C and isotopic fluid composition of 8.66–9.72‰. They were formed by crystallization of a highly evolved and sodic granitic magma. This study has implications for Central Brazil's economic potential and offers better understanding of tin behavior in rare, evolved peraluminous granitic magmas.

Keywords: albitite; snowball texture; Tin; rare metals; Ar-Ar age; oxygen isotope; Brazil

1. Introduction

Albitites are uncommon rocks with usually more than 70–80% of albite. Most of the known albitites worldwide have their origin attributed to the action of hydrothermal fluids on granites [1–3]. In this case, quartz and K-feldspar are leached by Na-rich fluids, in an albitization process, which is sometimes related to greisenization from evolved granites [4,5]. More rarely, albitites are formed by direct crystallization from Na-rich magmas, generally related to specialized and rare-metal granites [6–9]. This type can be recognized by typical textures, such as albite inclusions along growth planes in quartz or other mineral, called *snowball texture*, or the alignment of albite laths in the rock matrix, which is interpreted as flow texture. In addition to textural studies, geochemical characterization of associated granites is crucial to distinguish sodic enrichment in the magmatic stage from metasomatic enrichment [7,9–11].

This paper aims to study albitites that occur in a restricted area, i.e., the Goiás Tin Province, located in Central Brazil [12]. Albitites occur as possible dikes or lenses of 1 to 2.5 m thick, cutting

peraluminous granites and graphite schists, or as albitite lenses. They have economic and subeconomic tin concentrations. This led to the exploitation by artisanal miners and the interest of mining companies for mineral exploration in the 1980s. However, there was no mine installation in the area.

Geological Context

The study area is located within a region characterized by a geological evolution spanning from rhyacian to cryogenian times. In the region, there are schists and gneisses from the Paleoproterozoic Ticunzal Formation, the Aurumina Granitic Suite (2.17–2.12 Ga) [13–17], rift volcano-sedimentary rocks of the Araí Group, of ca. 1.77 Ga [12,18]; within-plate granites of the Goiás Tin Province, represented by the Pedra Branca Suite [9,12]; and Meso-Neoproterozoic sedimentary rocks of the Paranoá (1.2–0.9 Ga) and Bambuí groups (0.9–0.6 Ga; Figure 1A) [19]. The region was subjected to metamorphism and deformation in the Neoproterozoic (Brasiliano/Pan-African event).

The geological units identified in the study area are the Ticunzal Formation and the Aurumina Suite (Figure 1B). The Ticunzal Formation consists of graphite schist, mica-quartz schist, garnet-mica schist, and biotite gneiss. Its most striking feature is the presence of large amounts of graphite, which suggests a restricted marine sedimentary environment, warm and salt waters, with high biological activity. It is older than 2.17 Ga, the age of the oldest granitic intrusions of Aurumina Suite. Results of Sm-Nd isotopic data indicate model-age between 2.7 and 2.8 Ga for the metasedimentary package [13,20,21]. These lithologies are cut by granitic rocks attributed to the Aurumina Suite, which is generally divided in the following facies: muscovite granite, biotite-muscovite granite, tonalite, biotite granite and turmaline-muscovite granite. Pegmatites, albite granites and rare albitites are locally found. According to Botelho et al. [22], they are syn-collisional and S-type peraluminous Paleoproterozoic granites (2.12–2.17 Ga–zircon U-Pb), but recent data [14] show that the magmas of the Aurumina Suite were generated by the hybridization of mafic magmas and metasedimentary rocks, indicating that these peraluminous rocks are not true S-type granites.

This study was conducted in the Boa Vista and Pelotas artisanal mines. Geological, petrological and isotopic data from albitites and spatially associated-granites were integrated to constrain the genesis and evolution history of albitites. The study also intends to contribute to the literature on the petrogenesis and metallogenesis of evolved granitic systems rich in rare metals.

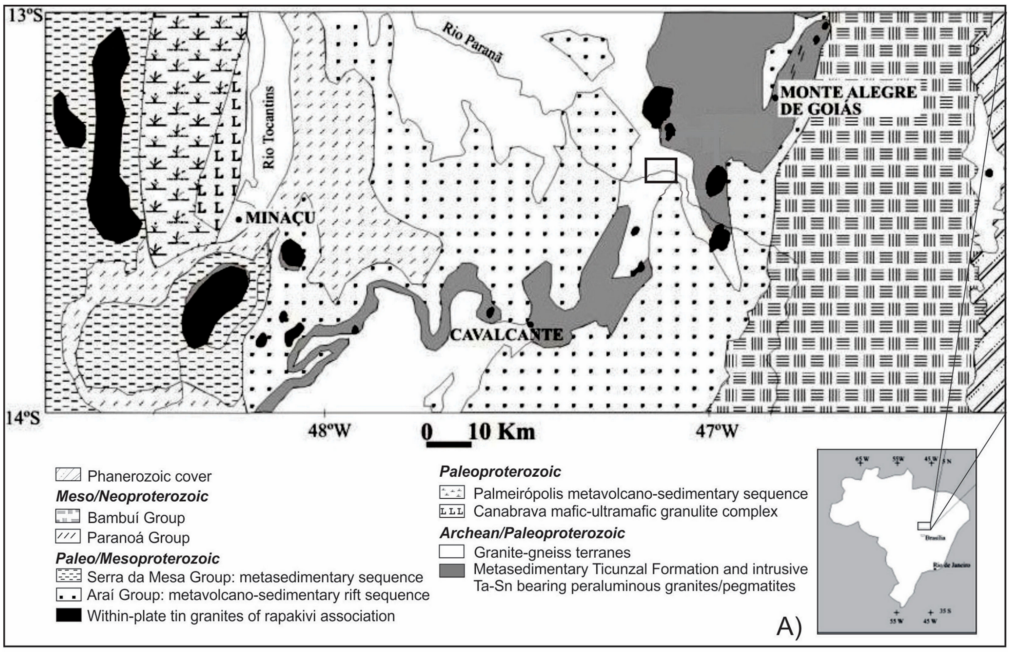

Figure 1. *Cont.*

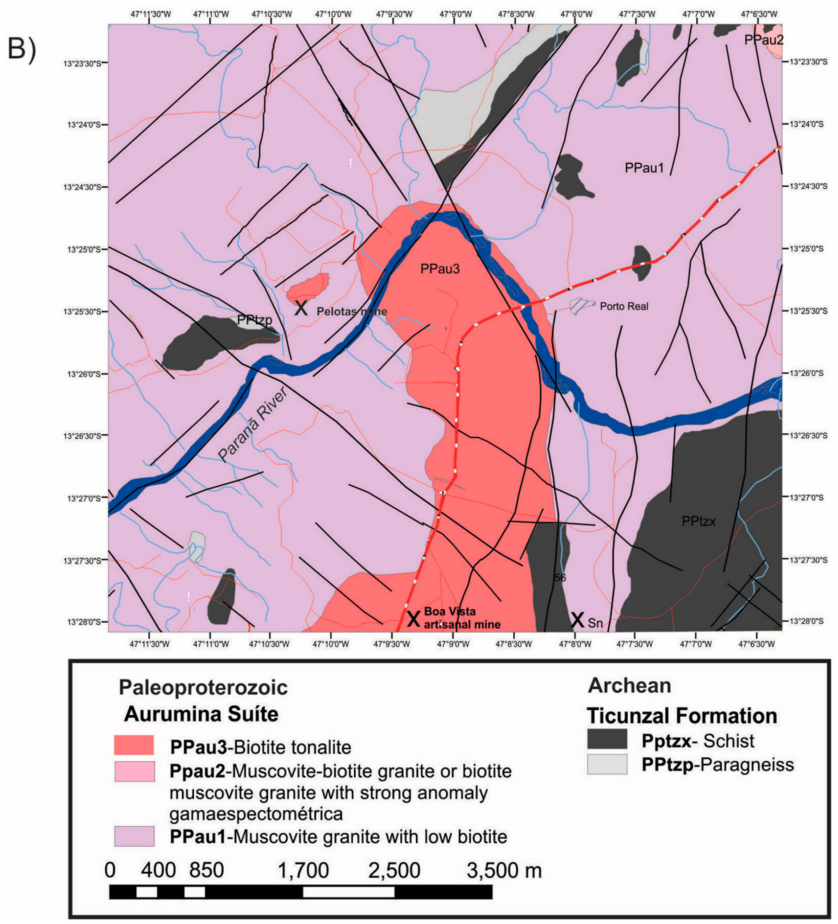

Figure 1. Geological sketch maps of the study area: (**A**) a map of the Goiás Tin Province, with inset showing the approximate region of the study area; and (**B**) a map showing the location of the Pelotas and the Boa Vista artisanal mines [23].

2. Materials and Methods

Two field trips for geological studies and sample collection occurred. Eight drill holes from the Pelotas artisanal mine were sampled. Eighty-six thin sections from selected samples were studied. The petrographic studies were conducted in the Microscopy Laboratory of the Geoscience Institute at the University of Brasilia. The chemical analyses were performed at Acme Analytical Laboratories Ltd. (Vancouver, BC, Canada). Major elements (SiO_2, TiO_2, Al_2O_3, Fe_2O_3, MnO, MgO, CaO, Na_2O, K_2O, P_2O_5) were analysed by ICP-ES (inductively coupled plasma-emission spectrometry). Trace elements (Be, Rb, Cs, Ba, Sr, Ca, V, Sn, W, Ta, Nb, Th, U, Zr, Hf, Y, Sc), including rare earth elements, were analysed by ICP-MS (inductively coupled plasma-mass spectrometry). Cr and Co were analysed by the Leco method.

Mineral chemistry data were obtained from JXA-8230-Jeol electron microprobe (Jeol, Peabody, MA, USA), in the Electronic Microprobe Laboratory of the Geoscience Institute at the University of Brasilia. The standards were commercially supplied by CAMECA.

The $^{40}Ar/^{39}Ar$ geochronological analysis was performed in the Isotope Laboratory at Queen's University, Department of Geological Sciences and Geological Engineering, Ontario (Kingston, ON, Canada). There, 23 temperature steps were performed in primary muscovite from albitite of the Boa Vista Artisanal Mine. Mica was irradiated for 40 h in a McMaster-type nuclear reactor. An 8 W Lexel 3500 specific ion laser (Ar), a MAP 216 mass spectrometer, with a *Baur-Signer* source, and an electron multiplier were used. The measurements of argon isotopes were normalized to atmospheric $^{40}Ar/^{36}Ar$ ratio, using the ratios proposed by [24]. Ages were calculated relative to Hb_3Gr (hornblende) with

assigned age of 1072 Ma [24] using conventional 40 K decay constants [25,26]. The analytical precision of individual steps for calculation of the plateau was 0.5% at 2σ level.

Stable isotope studies were performed on five samples of albitite, three on albitite from the Boa Vista Artisanal Mine and two on albitite from the Pelotas Artisanal Mine. Cassiterite and albite pairs were considered to be in paragenesis, based on petrographic study. The minerals were manually separated using a binocular loupe in the Geoscience Institute at the University of Brasilia: 5 mg of albite crystals and 3 mg of cassiterite crystals. The oxygen isotope analyses were performed in the laboratory of the Department of Geological Sciences and Geological Engineering at Queen's University (Kingston, ON, Canada). The oxygen isotopic compositions in albite and cassiterite pairs were measured using BrF_5 by the method of Clayton and Mayeda [27]. Measurements of stable isotopes were performed using a Finnigan MAT 252 mass spectrometer. All values are expressed in ‰. Results were presented as $\delta^{18}O$, relatively to the VSMOW standard (Vienna Standard Mean Ocean Water). The analytical precision was of ±0.3‰ for $\delta^{18}O$ values. The isotopic equilibrium temperature for the quartz-cassiterite and cassiterite-water pairs was calculated according to Zheng [28]. The equation used to calculate the isotopic equilibrium temperature for the albite-water system was proposed by Bottinga and Javoy [29].

3. Geological Setting and Textural Relationships of Albitites

The granitic rocks and albitites described in the studied area are attributed to the Aurumina Suite. The granitic rocks are mainly represented by muscovite-biotite monzogranite and tonalite. The field relationships between the granites could not be defined, as some were identified only in drill holes.

The studied albitites occur as lenses or dikes spatially associated to tonalites and monzogranites, which sometimes contain xenoliths of graphitic schists or even individual graphite lamellae interpreted as xenocrystic inclusions. Schists also occur in contact with both albitites and granitic rocks. They constitute biotite-chlorite-quartz-graphite schist with garnet and graphite-muscovite-chlorite schist (Figure 2A–F).

The muscovite-biotite monzogranite is whitish-gray, medium to coarse-grained, composed of quartz, plagioclase An_{22-1}, orthoclase, muscovite and biotite; chalcopyrite, pyrite, garnet ($Al_{80}Py_{12}Sp_4Gr_2$), and zircon are accessory minerals (Figure 2A,B,D). Tonalite is strongly altered near the albitites. It is whitish-grey to dark grey, composed of quartz (31–38%), altered plagioclase (48–58%), normally resulting in albite composition $An_{10-3\%}$, and microcline (3–5%) as essential minerals; biotite (1–2%) and muscovite (1–5%) as minor minerals (Figure 2E); and pyrite, chalcopyrite, zircon, and monazite as accessory minerals. Fine muscovite and zoisite/clinozoisite are the alteration minerals. Tonalites follow the modal criteria of classification from Streckeisen [30] nomenclature, and also the regional classification adopted by Botelho et al. [16] and Cuadros et al. [14].

Rare pegmatites and albite granite occur in the Pelotas Artisanal Mine, in contact with the granites and schists. They consist of quartz, K-feldspar, plagioclase, and muscovite.

Albitites from both the Boa Vista and the Pelotas artisanal mines are quite similar. In Pelotas, sharp contact between albitite and other rocks is identified in drill-holes (Figure 2F). Albitites are white isotropic rocks, consisting of albite (90–91%), quartz (3–3.5%), cassiterite (1–2%), apatite (1–2%), K-feldspar (0–1%), and primary muscovite (2–4%) (Figure 3A–E).

Albite occurs either as subhedral to euhedral grains, ranging from 0.3 to 1 mm in size, comprising alignment of albite laths, interpreted as flow texture (Figure 3F), or as 0.3 mm euhedral to subhedral laths included in cassiterite and apatite crystals (Figure 3C–E). These Type-2 inclusions of albite crystals arranged almost regularly along growth zones of cassiterite and apatite describe the texture classified as snowball [31] (Figure 3D). Based on textural criteria, albite is interpreted as being of magmatic origin.

Apatite forms subhedral grains 1 to 5.5 mm in size. It occurs as interstitial mineral in most cases. In general, it presents randomly arranged albite lath inclusions. In some crystals, albite is arranged parallel to the apatite border, forming a texture similar to snowball (Figure 3C). It has fluorapatite chemical composition, with low REE content. Cassiterite has euhedral to subhedral habit and ranges from 0.5 to 5.0 mm in size. The crystals are often twinned and the pleochroism varies from reddish

brown to yellowish brown. Type-2 albite inclusions are common, often forming snowball texture (Figure 3C,D). There are also inclusions of quartz and, more rarely, of muscovite.

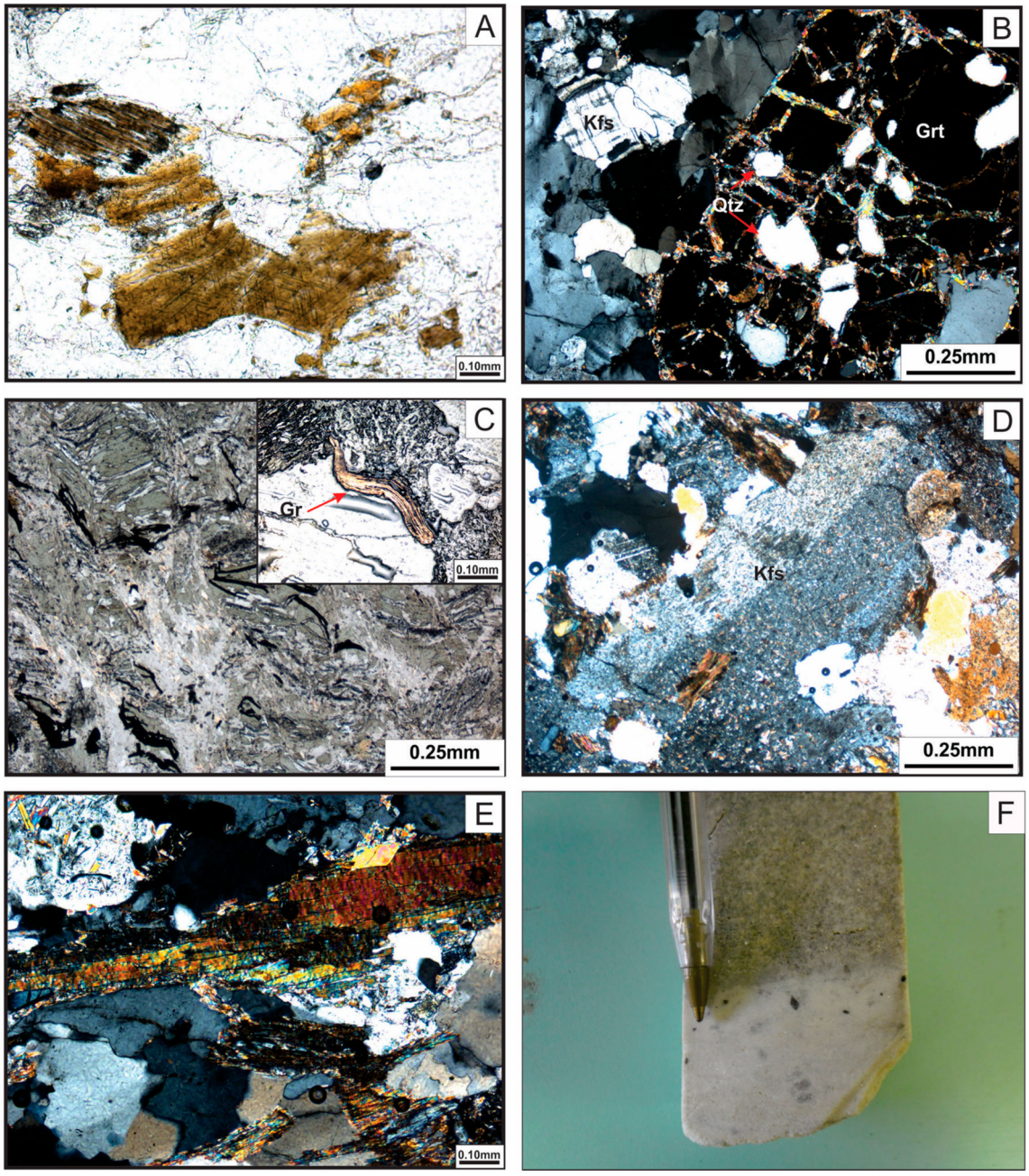

Figure 2. Photographs of representative rocks and features of the study area. (**A**) Coexisting garnet and biotite in muscovite-biotite monzogranite with garnet; (**B**) garnet phenocryst containing quartz inclusion in muscovite-biotite monzogranite with garnet; (**C**) textural aspect of the graphite-chlorite schist in reflected light, showing graphite lamellae; (**D**) altered orthoclase from biotite-muscovite monzogranite; (**E**) magmatic muscovite from biotite-muscovite tonalite; and (**F**) sharp contact between albitite and monzogranite. Kfs: K-feldspar; Grt: garnet; Qtz: quartz; Gr: graphite.

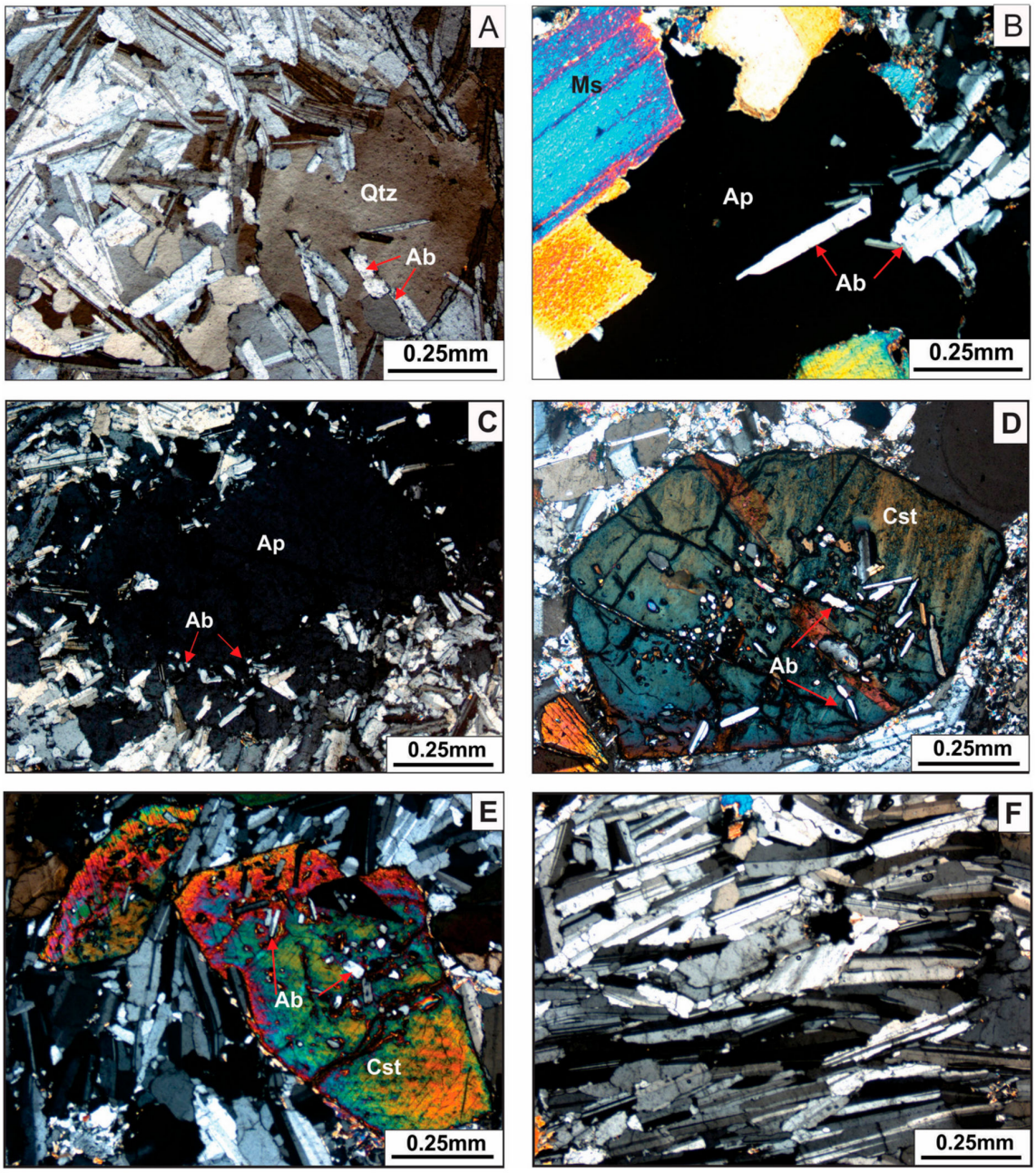

Figure 3. Representative photomicrographs showing textural features of albitites from the Boa Vista and Pelotas artisanal mines. (**A**) Quartz crystals with albite lath inclusions; (**B**) interstitial apatite with albite inclusions in reentrant contact with magmatic muscovite; (**C**) magmatic apatite crystal containing albite inclusions interpreted to be along apatite growth zones; (**D**) cassiterite with albite lath inclusions in the core, forming snowball texture; (**E**) cassiterite with albite lath inclusions and contact relationship with albite from the rock matrix; and (**F**) alignment of albite laths. Ab: albite; Ap: apatite; Cst: cassiterite; Ms: muscovite; Qtz: quartz.

4. Results

4.1. $^{40}Ar/^{39}Ar$ *Age*

$^{40}Ar/^{39}Ar$ data were obtained for magmatic muscovite of the albitite from Boa Vista Artisanal Mine. In order to estimate age of the crystalization, 23 increment temperature steps were run.

The obtained age spectrum show a staircase pattern. The first step accounts only for 3.5% of ^{39}Ar released and yields an age of 618.0 ± 36.2 Ma. The high temperature steps yield a plateau-like pattern, which accounts for 47.8% of ^{39}Ar, with the mean age of 1996.6 ± 13.0 Ma (MSWD = 0.983), near the integrated age of 1957.18 ± 11.15 Ma (Figure 4). Typical criteria to define the plateau age are: (1) the plateau region of age spectrum with at least 70% of total ^{39}Ar released; (2) at least three steps on the plateau; and (3) the individual ages of these steps must agree with each other within analytical error (e.g., Corsini et al. [32]). The dated sample do not fit two these criteria by the amount of ^{39}Ar released. Thus, we interpret the age of 1996.6 ± 13.0 Ma as approaching the muscovite crystallization age, but not necessarily reflecting the true crystallization age of albite due to partial resetting at the regional metamorphism during the Brasiliano (Pan-African) event. The lowest age of 618.0 ± 36.2 Ma may directly correspond to this metamorphism. Obviously, the crystallization of the albitite is equal, or older, than the mean age of the plateau-like steps (~2.0 Ga) and may be younger, or equal, to the age of Paleoproterozoic Aurumina granites (~2.12–2.17 Ga).

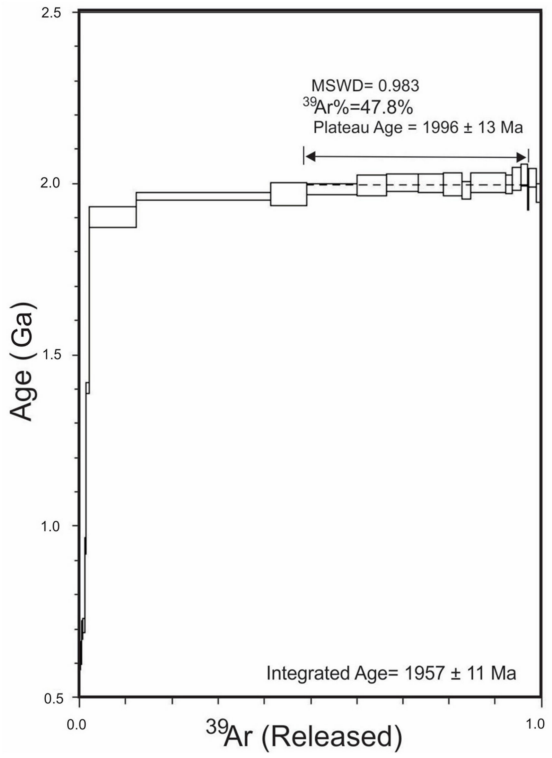

Figure 4. Results of ^{40}Ar/^{39}Ar obtained in primary muscovite from the Boa Vista albitite, showing the plateau age, interpreted as approaching the muscovite crystallization age.

4.2. Lithogeochemistry

The chemical representative compositions of the studied rocks are shown in Table 1 and Figures 5 and 6. For comparison, an analysis of a tourmaline-albite granite (TAG) described by Cuadros et al. [14] near the region of the studied albitites was added to Figure 5. According to the Alumina Saturation Index (ASI = $Al_2O_3/CaO + Na_2O + K_2O$ − molar; [33]), albite granites, monzogranites and tonalites are classified as peraluminous rocks (ASI = 1.1 to 1.8), while albitites are classified as metaluminous to peraluminous (ASI = 0.8 to 1.3; Figure 5A). Albitites with lower SiO_2 content show ASI varying from 0.8 to 0.95, and albitites with higher SiO_2 content present ASI ranging from 1.1 to 1.25. These higher ASI values can be explained by the increased amount of muscovite in some samples. Albitite samples richer in muscovite and quartz and poorer in albite and apatite presents higher K_2O and SiO_2 and less Na_2O, CaO, and P_2O_5 contents (Table 1).

Table 1. Representative whole-rock chemical analysis of the studied rocks (wt %).

Rock	Albitite				Tonalite		Schist	Monzogranite							
%															
SiO_2	70.5	71.25	75.9	70.5	74.38	74.9	49.83	75.3	73.6	74.4	75.9	73.5	70.9	75.2	74.1
TiO_2	<0.01	<0.01	0.04	0.01	0.02	0.02	0.8	0.14	0.12	0.13	0.14	0.15	0.3	0.05	0.11
Al_2O_3	17.1	16.83	14.3	15	16.25	15.5	23.58	14.3	14.5	14.3	13.5	14.6	14.4	14.1	14.4
Fe_2O_3	0.1	0.15	0.27	0.22	0.36	0.35	9.19	0.79	1.15	1.21	1.09	1.51	2.45	0.62	1.22
MnO	0.01	0.06	0.01	0.05	<0.01	<0.01	0.27	<0.01	<0.01	0.01	<0.01	0.02	0.02	<0.01	0.01
MgO	<0.01	<0.01	0.06	0.04	0.08	0.1	2.21	0.25	0.24	0.27	0.28	0.34	0.81	0.13	0.26
CaO	1.07	0.53	0.36	2.46	0.71	0.6	2.35	0.46	1.35	1.56	0.89	1.54	1.13	1.12	1.47
Na_2O	9.59	9.86	6.6	8.08	4.79	5.12	2.49	3.76	4.29	3.95	4.03	3.68	3.23	3.66	3.89
K_2O	0.06	0.1	0.88	0.54	2.04	1.73	4.55	3.78	3.58	3.06	2.98	3.43	5.09	4.18	3.29
P_2O_5	0.78	0.43	0.26	1.82	0.07	0.06	0.11	0.07	0.06	0.88	0.09	0.1	0.3	0.09	0.07
LOI	0.7	0.6	0.9	0.8	1.2	1.5	4.3	1.1	0.9	1.0	1.0	1.0	1.1	0.7	1.0
TOTAL	99.9	99.83	99.5	99.6	99.85	99.9	99.72	99.9	99.9	99.9	99.9	99.9	99.8	99.9	99.9
ppb															
Au	<0.5	0.5	<0.5	0.6	1.1	0.8	0.7	<0.5	<0.5	<0.5	1.3	<0.5	0.8	1	1.3
ppm															
Be	31	148	4	4	4	<1	14	4	11	15	4	8	8	<1	8
Rb	1.5	2.5	282	33.4	63.8	57.1	219	157	101	96	115	124	142	114	107
Cs	0.2	2.8	84.6	1.9	10.4	9.5	28.7	9.3	6.4	6.8	9.9	6.8	13.4	2.9	7.7
Ba	3	7	49	31	602	526	701	311	352	259	353	352	1022	394	321
Sr	115	75.3	33.4	139	289.7	265	378.6	78.6	187	152	183	169	145	152	198
Ga	15.7	13.4	15.4	14	13.3	111	28.7	15.7	15.3	17	13	16.8	17	14.9	14.1
V	21	27	21	23	32	33	146	41	36	27	30	31	57	46	46
Sn	8	398	3218	2851	11	11	4	5	2	1	3	5	4	2	1
W	<0.5	<0.5	2	0.9	1.5	1.4	4.1	0.6	<0.5	<0.5	<0.5	<0.5	0.7	<0.5	<0.5
Ta	1.7	18.7	24.2	111	0.1	<0.1	0.9	0.5	0.2	0.2	0.2	0.8	0.6	0.2	0.3
Nb	1.3	12.9	12	72.2	0.6	0.7	11.9	3.8	3.1	3.3	2.2	4.6	5	1.7	3.1
Th	0.5	<0.2	0.9	0.2	2.8	0.4	17.5	8	6.3	7.4	10.5	5.5	6.1	2.8	5.2
U	2.8	0.8	1.5	6.2	<0.1	0.2	4.3	2.4	4	6.3	3.9	5.5	4.4	2.1	2.3
Zr	15.5	21.5	36.3	16.1	1.2	5.5	189.1	70.7	68.6	82.1	114	76.7	90.6	32	58.4
Hf	1.4	2.9	3.3	2.6	<0.1	<0.1	4.6	2.1	2.1	1.9	3.4	2	2.3	1.1	1.4
Y	2	0.1	1.6	4	0.4	0.9	34.9	2.1	2.2	4	3.7	3.4	6.9	3.8	3.1
Sc	<1	<1	<1	<1	<1	<1	23	1	1	2	2	2	3	1	1
La	0.9	0.2	2.7	2.3	3.4	2.7	57.9	16.5	14.9	15.5	22.5	13.4	22	8.2	12.8
Ce	1.7	0.2	4.3	4.5	4.9	5.3	117.7	28.7	26.2	27.1	39	27.2	42.4	15.8	23.7
Pr	0.16	<0.02	0.44	0.46	0.52	0.52	12.96	2.79	2.38	2.51	3.91	2.68	4.36	1.55	2.31
Nd	1.2	<0.3	1.6	0.9	1.2	1.6	46.4	9.2	7.6	8.3	13.3	8.1	15.4	5.6	7.1
Sm	0.21	<0.05	0.26	0.69	0.19	0.24	9.03	1.55	1.42	1.6	2.48	1.81	2.85	1.32	1.41
Eu	0.12	<0.02	0.09	0.27	0.9	0.87	1.72	0.44	0.54	0.44	0.55	0.56	0.74	0.53	0.57
Gd	0.22	<0.05	0.3	0.97	0.2	0.32	7.43	1.23	0.98	1.25	1.8	1.67	2.39	1.1	1.27
Tb	0.06	<0.01	0.05	0.28	0.03	0.03	1.11	0.14	0.14	0.18	0.23	0.21	0.33	0.18	0.16
Dy	0.19	<0.05	0.3	1.11	0.09	0.11	7.08	0.6	0.42	0.83	0.98	0.97	1.37	0.93	0.63
Ho	<0.02	<0.02	0.05	0.09	0.03	0.02	1.37	0.08	0.08	0.21	0.13	0.13	0.28	0.18	0.16
Er	0.05	<0.03	0.06	0.07	<0.03	<0.03	4.09	0.1	0.16	0.27	0.23	0.22	0.44	0.35	0.26
Tm	0.02	<0.01	<0.01	0.01	<0.01	<0.01	0.61	0.01	0.03	0.03	0.03	0.03	0.08	0.05	0.03
Yb	0.07	<0.05	<0.05	<0.05	<0.05	0.09	3.96	0.1	0.09	0.12	0.35	0.24	0.51	0.13	0.17
Lu	<0.01	<0.01	<0.01	<0.01	0.02	0.02	0.59	0.03	0.03	0.04	0.03	0.03	0.06	0.05	0.02
Ni	0.1	0.5	<0.1	<0.1	0.2	0.3	42.1	<0.1	0.6	0.9	0.9	0.6	6.8	<0.1	0.6
Cr	<20	<20	<20	<20	<20	<20	116.3	<20	<20	<20	27.4	<20	20.5	<20	<20
Co	<0.2	<0.2	0.4	0.3	0.7	0.5	21.6	1.1	1.4	1.8	2	2.3	5	1.1	1.4
Cu	1.3	1.7	0.5	1.2	1.2	1.4	73.2	1.7	2.7	0.9	1.9	1.3	9.2	1.4	1.7
Cd	<0.1	<0.1	0.1	2.1	<0.1	<0.1	<0.1	<0.1	<0.1	<0.1	<0.1	<0.1	<0.1	<0.1	<0.1
Zn	10	3	4	14	<1	<1	97	6	19	20	18	18	63	3	13
Pb	4	0.6	3.8	8.5	22.7	25.8	5.5	6.6	9.6	6.3	11.8	29.9	37.8	6.6	5.1
Mo	<0.1	0.1	<0.1	<0.1	<0.1	<0.1	0.7	<0.1	<0.1	<0.1	<0.1	<0.1	0.4	<0.1	<0.1
Ag	<0.1	<0.1	<0.1	<0.1	<0.1	<0.1	<0.1	<0.1	<0.1	<0.1	<0.1	0.2	0.1	<0.1	<0.1
As	<0.5	<0.5	<0.5	<0.5	0.6	<0.5	3	<0.5	<0.5	<0.5	1.3	0.6	1.4	<0.5	<0.5
Sb	<0.1	<0.1	<0.1	<0.1	<0.1	<0.01	<0.1	<0.1	<0.1	<0.1	<0.1	<0.1	<0.1	<0.1	<0.1
Bi	<0.1	<0.1	<0.1	<0.1	1.9	0.8	0.1	<0.1	<0.1	0.1	0.1	0.3	0.3	<0.1	<0.1
Se	<0.5	<0.5	<0.5	<0.5	<0.5	<0.5	<0.5	<0.5	<0.5	<0.5	<0.5	<0.5	<0.5	0	<0.5
Hg	0.03	<0.01	<0.01	<0.01	<0.01	<0.01	<0.01	<0.01	<0.01	<0.01	<0.01	<0.01	<0.01	<0.01	<0.0
Tl	<0.1	<0.1	0.2	<0.1	<0.1	<0.1	0.2	<0.1	0.2	0.1	0.2	0.1	0.4	<0.1	0.2

Albitites display high contents of Na_2O, Al_2O_3, P_2O_5, Sn, Ta, and Nb (Ta > Nb), and low contents of K_2O, TiO_2, Fe_2O_3, MgO, CaO, Ba, Sr, Zr, Th, and Rb. Compared with albitites, albite granites have higher contents of K_2O, Ba, and Sr and lower contents of Na_2O, CaO, P_2O_5, Sn, Ta, Nb, and Zr. Compared with albitites and albite granites, monzogranites are enriched in TiO_2, Fe_2O_3, MgO, K_2O,

Th, Rb, and Zr; depleted in Na_2O, P_2O_5, Al_2O_3, Sn, Nb and Ta (Nb > Ta); and they have intermediate contents of Sr and Ba. The analysed tonalite have intermediate levels of Fe_2O_3, MgO, K_2O, Na_2O ($Na_2O > K_2O$), and CaO; high contents of Al_2O_3, Ba, and Sr; and low contents of TiO_2, P_2O_5, Zr, Rb, Sn, Nb, Ta (Nb > Ta), and Th (Figure 6). The content of U in all the analysed rocks is low (<7 ppm; Table 1). MgO/TiO_2 average ratios are 3.6 and 2.2 for tonalites and monzogranites, respectively (Table 1; Figures 5B,C and 6).

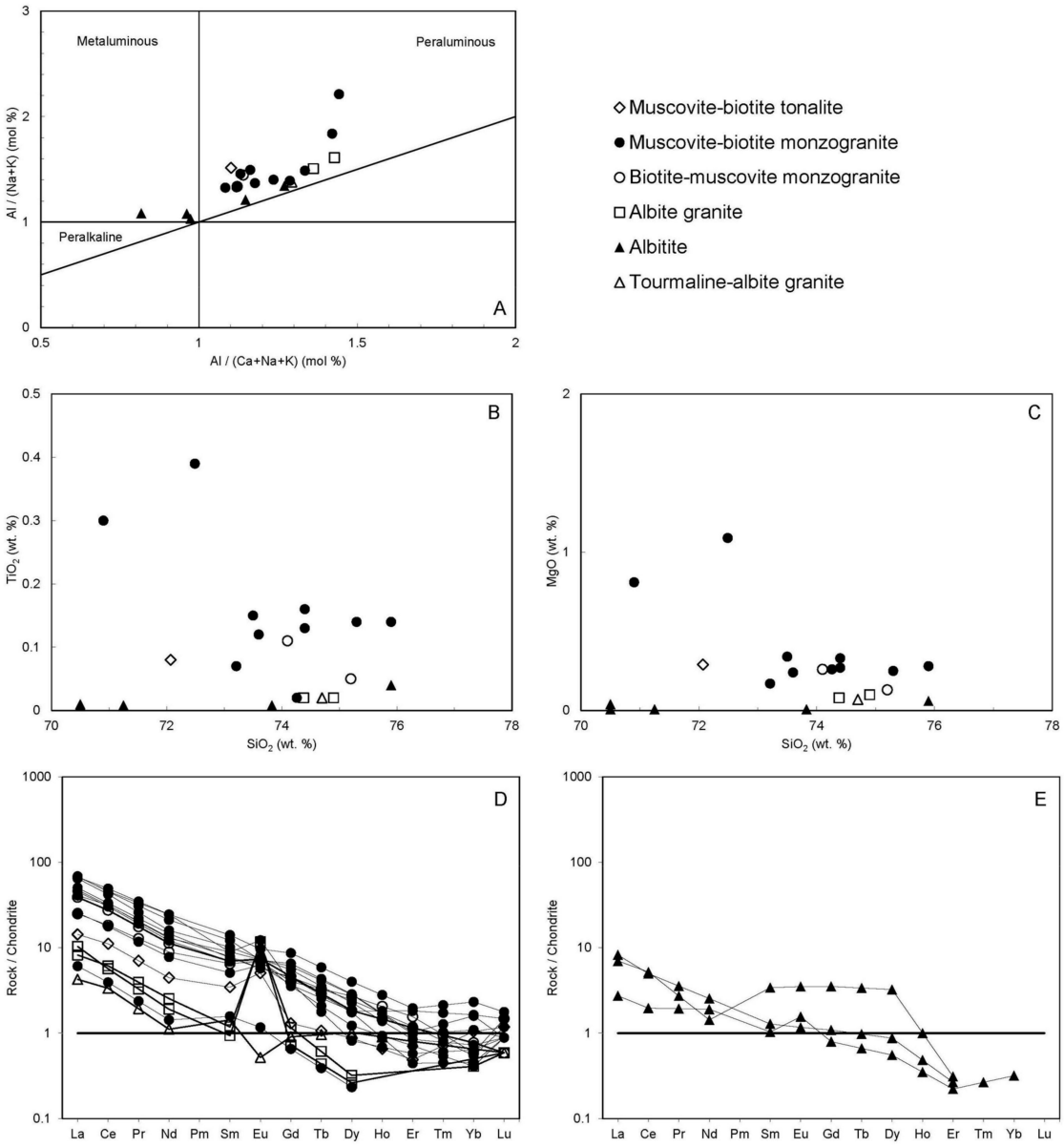

Figure 5. Representative diagrams of compositional characteristics of granites and albitites. (**A**) Classification based on Shand index in Maniar and Piccoli diagram [33], showing the peraluminous character of tonalite, monzogranites and albite granites, and the metaluminous to peraluminous character of albitites from the Pelotas and the Boa Vista artisanal mines; (**B**) $TiO_2 \times SiO_2$ diagram; (**C**) $MgO \times SiO_2$ diagram; (**D**) REE patterns of tonalite, monzogranites and albite granites normalized to chondrite, using Nakamura [34] values; and (**E**) REE patterns of albitites normalized to chondrite using Nakamura [34] values. Tourmaline-albite granite (TAG) sample from Cuadros et al. [14] was added to the diagrams.

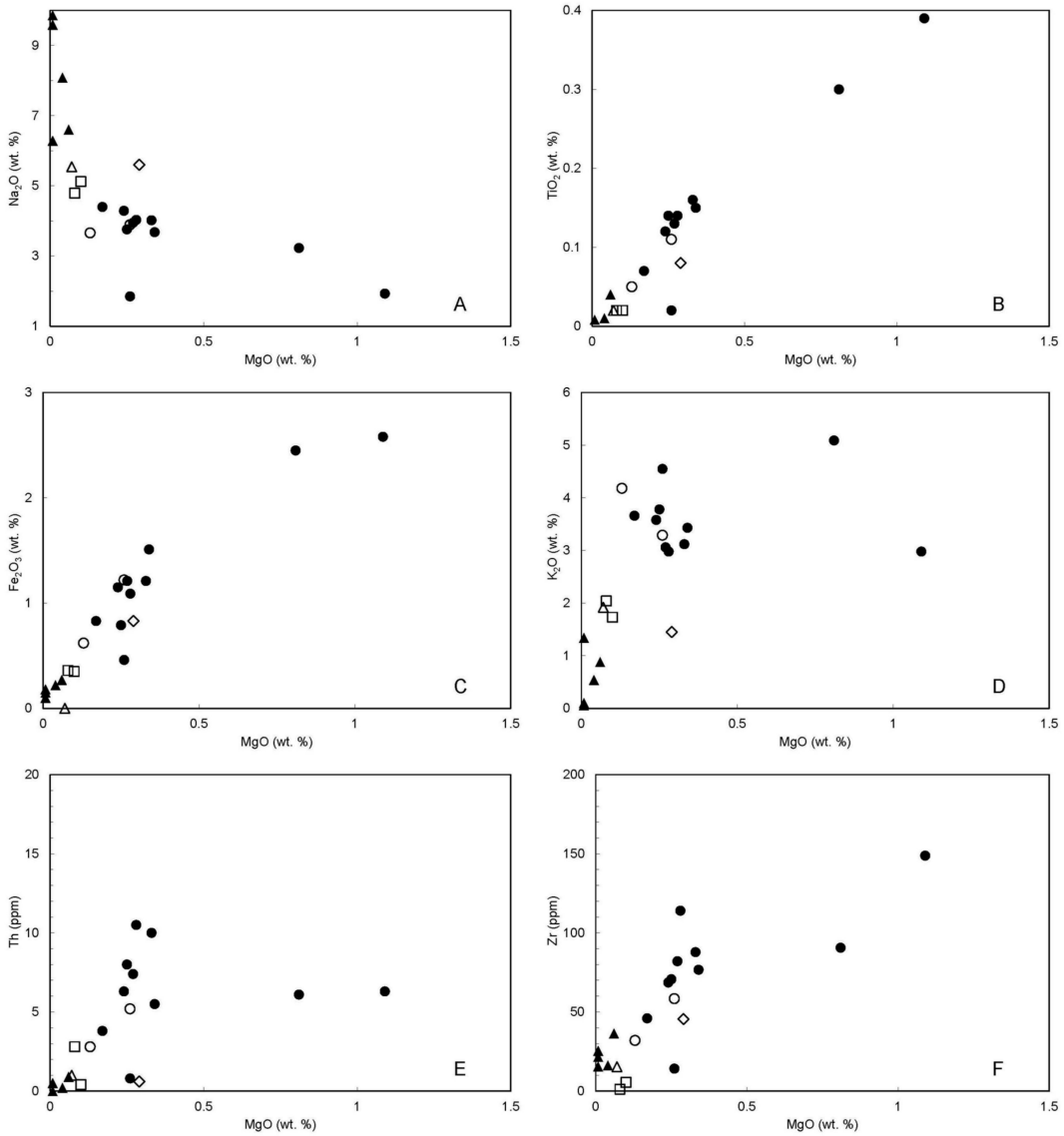

Figure 6. Variation diagrams for monzogranite, tonalite and albitite samples from the Pelotas and the Boa Vista artisanal mines. (**A**) MgO × Na_2O diagram; (**B**) MgO × TiO_2 diagram; (**C**) MgO × Fe_2O_3 diagram; (**D**) MgO × K_2O diagram; (**E**) MgO × Th diagram (**F**) MgO × Zr diagram. Legend as in Figure 5.

The values of rare earth elements (ΣREE) are low in all felsic rocks, in contrast to the schists values. They range from 0.4 to 11.6 ppm in albitites, from 11.5 to 11.6 ppm in albite granites, from 35–93 ppm in monzogranites, and reach 20.3 ppm in the tonalite (Table 1). The REE patterns normalized to the Nakamura [34] chondrite values for monzogranites (Figure 5D) are enriched in light rare earth elements (LREE) and depleted in heavy rare earth elements (HREE). Eu anomalies range from slightly positive to negative (0.99 < Eu/Eu* < 1.44). The patterns are slightly to strongly fractionated (La_n/Yb_n = 15.6 to 110.7). For albite granites, the REE patterns are enriched in LREE as opposed to HREE, whose concentrations are below or near the detection limit of the anlytical method (Table 1). They have a pronounced positive Eu anomaly (Eu/Eu* = 2–14), and their REE patterns are strongly fractionated (La_n/Yb_n ranges from 20 to 106; Figure 5D). Albitites do not follow the same REE pattern (Figure 5E). There is a slight enrichment in LREE compared to HREE (La_n/Yb_n ranges from 2.6 to 30). The Eu anomalies are absent or very discrete, and slightly positive (Eu/Eu* = 1 to 1.7).

4.3. Mineral Chemistry

Plagioclase chemical composition in the analysed rocks varies from albite to albite-oligoclase (Figure 7A). Albite ($Ab_{90-99}An_{10-0,6}Or_{0,4}$) occurs in albitites and muscovite-biotite tonalite facies. It contains Na_2O values between 12% and 13 wt % in albitites and between 10.5% to 11.9% in the muscovite-biotite tonalite facies. CaO contents are between 0.1% and 0.6 wt %, and 0.5% and 2.8% in albitites and tonalites, respectively.

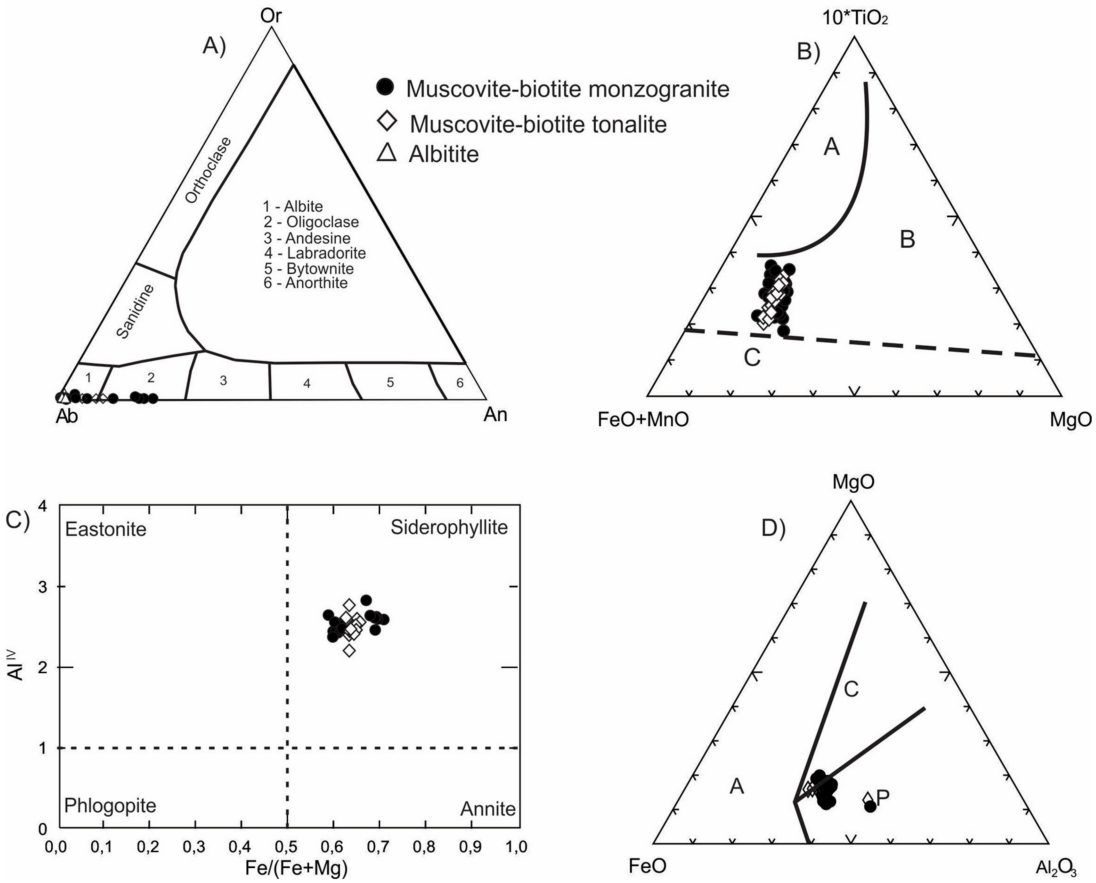

Figure 7. Chemical composition diagrams of plagioclase and biotite of tonalite, monzogranite, and albitite. (**A**) Classification diagram of the analysed plagioclase; (**B**) (FeO + MnO) − ($10*TiO_2$) − MgO diagram of Nachit et al. [35], showing the compositional variations of the analysed biotite (A = field of primary magmatic biotite; B = field of magmatic reequilibrated biotite; C = field of secondary biotite); (**C**) Al^{IV} vs. Fe/(Fe + Mg) diagram, proposed by Deer et al. [36]; and (**D**) the relationship between MgO-Al_2O_3, $FeO_{(t)}-Al_2O_3$, $MgO-FeO_{(t)}$, and $MgO-FeO_{(t)}-Al_2O_3$ for the biotite from monzogranites and tonalites in the diagram proposed by Abdel-Rahman [37] (A = alkali granites; C = calc-alkaline granites; P = peraluminous granites).

Albite from albitites has a more sodic composition, with Ab = 96–99%. The albite molecule in albite of muscovite-biotite tonalite has Ab = 90–97%, revealing little less sodic compared to albitites.

The muscovite-biotite monzogranite has plagioclase with albite-oligoclase composition ($Ab_{77-99}An_{22-1}Or_1$; Figure 7A). It presents Na_2O values between 9.2% and 12.3% and CaO values between 0.1 and 4.8%. In grains where there is a compositional variation, the core is more calcic than the rim.

According to the triangular diagram $10*TiO_2$ vs. FeO + MnO vs. MgO [35], the different biotite types are positioned in the reequilibrated magmatic biotite field (Figure 7B). The TiO_2 content is between 0.8 and 1.7%, MgO content generally ranges from 6 to 9.5%, while the values of Al_2O_3, from 17

to 19% (Table 2). The biotite of monzogranite and tonalite is classified as siderophyllite in the Mg/(Mg + Fe) vs. Al^{IV} diagram proposed by Deer et al. [36]; Figure 7C). The Fe/(Fe + Mg) ratio is between 0.58 to 0.71 apfu, and the content of Al^{IV} varies from 2.1 to 3.3 apfu. The average chemical formula can be defined as: $(K_{1.82},Na_{0.02},Ca_{0.01})_{1.85}$ $(Fe_{3.06},Mg_{1.75},Al^{VI}{}_{0.69},Ti_{0.14},Mn_{0.03})_{5.71}$ $Si_{5.44}Al^{IV}{}_{2.56}O_{20}(OH_{3.7}F_{0.3})_4$.

Table 2. Representative analyses of muscovite, biotite, and cassiterite from the studied rocks (wt %).

	Muscovite				Biotite					Cassiterite			
	Albitite		Tonalite		Tonalite		Monzogranite			Boa Vista Albitite		Pelotas Albitite	
	S	P	S	P						N	B	N	B
SiO_2	47.70	48.40	48.77	47.36	36.04	35.61	35.84	36.05	SiO_2	0.03	0.00	0.00	0.10
TiO_2	0.02	0.07	0.15	0.28	1.10	1.20	1.41	0.96	Al_2O_3	0.00	0.00	0.00	0.02
Al_2O_3	33.79	33.67	33.60	34.67	17.65	17.47	17.91	17.76	FeO	0.10	0.25	0.12	0.24
FeO	0.93	0.86	2.50	1.85	23.04	23.45	22.92	22.51	MnO	0.02	0.03	0.00	0.03
MnO	0.06	0.02	1.19	0.12	0.29	0.10	0.15	0.25	WO_3	0.00	0.00	0.00	0.00
MgO	0.02	0.11	0.05	1.06	7.48	8.11	8.08	8.08	As_2O_5	0.00	0.00	0.00	0.00
CaO	0.06	0.00	0.04	0.00	0.02	0.07	0.30	0.05	Ta_2O_5	0.45	0.96	0.48	0.73
Na_2O	0.88	0.68	0.27	0.30	0.05	0.08	0.04	0.21	Sb_2O_5	0.38	0.46	0.35	0.36
K_2O	10.56	10.23	10.67	10.60	9.65	9.56	9.28	9.47	SO_3	0.00	0.01	0.00	0.00
SrO	0.11	0.00	0.00	0.05	0.03	0.00	0.02	0.00	Bi_2O_3	0.00	0.00	0.00	0.00
BaO	0.02	0.00	0.06	0.00	0.26	0.00	0.01	0.00	Nb_2O_5	0.11	0.38	0.22	0.66
F	0.00	0.00	0.38	0.32	0.62	0.27	0.30	0.29	In_2O_3	0.17	0.13	0.12	0.17
Cl	0.00	0.00	0.01	0.00	0.03	0.03	0.03	0.04	SnO_2	99.32	98.30	99.31	97.74
H_2O *	4.46	4.49	4.38	4.39	3.61	3.77	3.79	3.78	UO_2	0.00	0.02	0.00	0.00
Total	98.61	98.58	101.90	100.86	99.66	99.65	99.98	99.40	CuO	0.00	0.01	0.02	0.00
FORMULE ON THE BASIS OF 22O									ZnO	0.00	0.00	0.00	0.01
Si	6.409	6.470	6.406	6.249	5.524	5.466	5.453	5.510	TOTAL	100.57	100.55	100.63	100.05
Al^{iv}	1.591	1.530	1.594	1.751	2.476	2.534	2.547	2.490	FORMULE ON THE BASIS OF 2O				
Site T	8	8	8	8	8	8	8	8	Si	0.001	0.000	0.000	0.002
Al^{vi}	3.760	3.775	3.609	3.640	0.712	0.628	0.666	0.710	Al	0.000	0.000	0.000	0.000
Ti	0.002	0.007	0.015	0.028	0.126	0.138	0.162	0.110	Fe	0.002	0.005	0.003	0.005
Fe	0.105	0.096	0.274	0.204	2.953	3.011	2.916	2.878	Mn	0.001	0.001	0.000	0.001
Mn	0.003	0.003	0.132	0.014	0.038	0.013	0.019	0.032	W	0.000	0.000	0.000	0.000
Mg	0.007	0.021	0.011	0.208	1.708	1.857	1.832	1.840	As	0.000	0.000	0.000	0.000
Site M	3.876	3.907	4.040	4.094	5.538	5.647	5.594	5.570	Ta	0.003	0.007	0.003	0.005
Ca	0.008	0.001	0.006	0.000	0.003	0.012	0.049	0.007	Sb	0.003	0.004	0.003	0.003
Na	0.229	0.176	0.068	0.076	0.016	0.024	0.013	0.063	Nb	0.001	0.004	0.003	0.008
K	1.810	1.744	1.788	1.784	1.886	1.872	1.802	1.847	In	0.002	0.001	0.001	0.002
Sr	0.009	0.000	0.000	0.004	0.003	0.000	0.001	0.000	Sn	0.987	0.977	0.986	0.973
Ba	0.001	0.000	0.003	0.000	0.015	0.000	0.001	0.000	U	0.000	0.000	0.000	0.000
Site I	2.057	1.921	1.866	1.864	1.926	1.911	1.867	1.924	Cu	0.000	0.000	0.000	0.000
OH *	4.000	4.000	3.842	3.866	3.691	3.862	3.851	3.853	Zn	0.000	0.000	0.000	0.000
F	0.000	0.000	0.157	0.134	0.301	0.130	0.142	0.138	TOTAL	1.000	0.999	1.000	1.000
Cl	0.000	0.000	0.001	0.000	0.009	0.008	0.006	0.009					
Site A	4	4	4	4	4	4	4	4					
TOTAL	31.867	31.656	31.812	31.915	35.905	35.940	35.823	35.964					

* Calculated values; S = Secondary mineral; P = Primary mineral; N = Nucleus; B = Border.

In tectonic discrimination diagrams proposed by Abdel-Rahman [37], the biotite analyses of monzogranite and tonalite are located predominantly in the biotite field of peraluminous granitic suites (Figure 7D).

Muscovite with textural characteristics of primary muscovite has variation in the chemical composition between biotite-muscovite tonalite and albitite (Table 2). The muscovite from biotite-muscovite tonalite has the following composition: SiO_2 = 45.43–49.50%, Al_2O_3 = 32.58–38.75%, FeO (t) = 0.54–3.70%, TiO_2 = 0.0–1.15%, MgO = 0.04–1.07%, MnO = 0.0–1.8%, K_2O = 10.11–11.24%, Na_2O = 0.20–0.69%, and CaO = 0.0–0.08%. The muscovite from albitites has the following content: SiO_2 = 45.26–48.40%, Al_2O_3 = 26.28–33.99%, FeO (t) = 0.20–3.40%, TiO_2 = 0.0–0.07%, MgO = 0.0–0.93%, MnO = 0.0–0.15%, K_2O = 9.20–10.89%, Na_2O = 0.26–0.96%, and CaO = 0.0–0.17%. It has mostly no fluorine and chlorine.

Primary muscovite of tonalite differs from the secondary one for having higher Al, Mg, and Na contents and lower Fe and Si contents (Table 2; Figure 8). In relation to Ti concentrations, usually used to distinguish primary (high Ti) from secondary (low Ti) muscovite [38,39], analyses of magmatic muscovite of tonalite displayed different contents of titanium, apparently contradicting the textural

interpretation. On the other hand, the muscovite petrographically interpreted as secondary always has low TiO_2 (0.0–0.02 apfu) contents (Figure 8A). With the exception of Ti content, the chemical composition of primary muscovite of tonalite follows the conclusions of Miller et al. [38], according to whom crystals that have the textural aspect of primary muscovite have typically higher Ti, Na, and Al contents and lower Si and Mg contents compared with secondary muscovite.

All analyses of muscovite of albitites had almost zero Ti contents, and low Mg and Fe contents. In contrast, both the primary and the secondary muscovite of albitite have high Na, Al and Si contents (Table 2; Figure 8).

The results made it possible to conclude that the combination of textural and compositional characteristics should be used to distinguish primary from secondary muscovite. Similar conclusions were obtained by Zane and Rizzo [40] and Tao et al. [41]. The chemical composition of the studied rocks is interpreted to have acted as a control factor on the composition of primary muscovite, especially in Na_2O and TiO_2 contents.

Cassiterite with textural characteristics of primary mineral from albitites of the Boa Vista and Pelotas artisanal mines were analysed. In general, the reddish-brown portions have higher SnO_2 contents and lower FeO, Ta_2O_5, and Nb_2O_5 contents (Ta > Nb) for both areas. The opposite occurs in bands with light brown pleochroism (Figure 9). In cassiterite from Boa Vista, this pattern is more evident than in cassiterite from the Pelotas mine. In crystals without zonation, the nucleus is generally richer in Sn and poorer in Ta, Nb, and Fe in comparison with the border (Table 2).

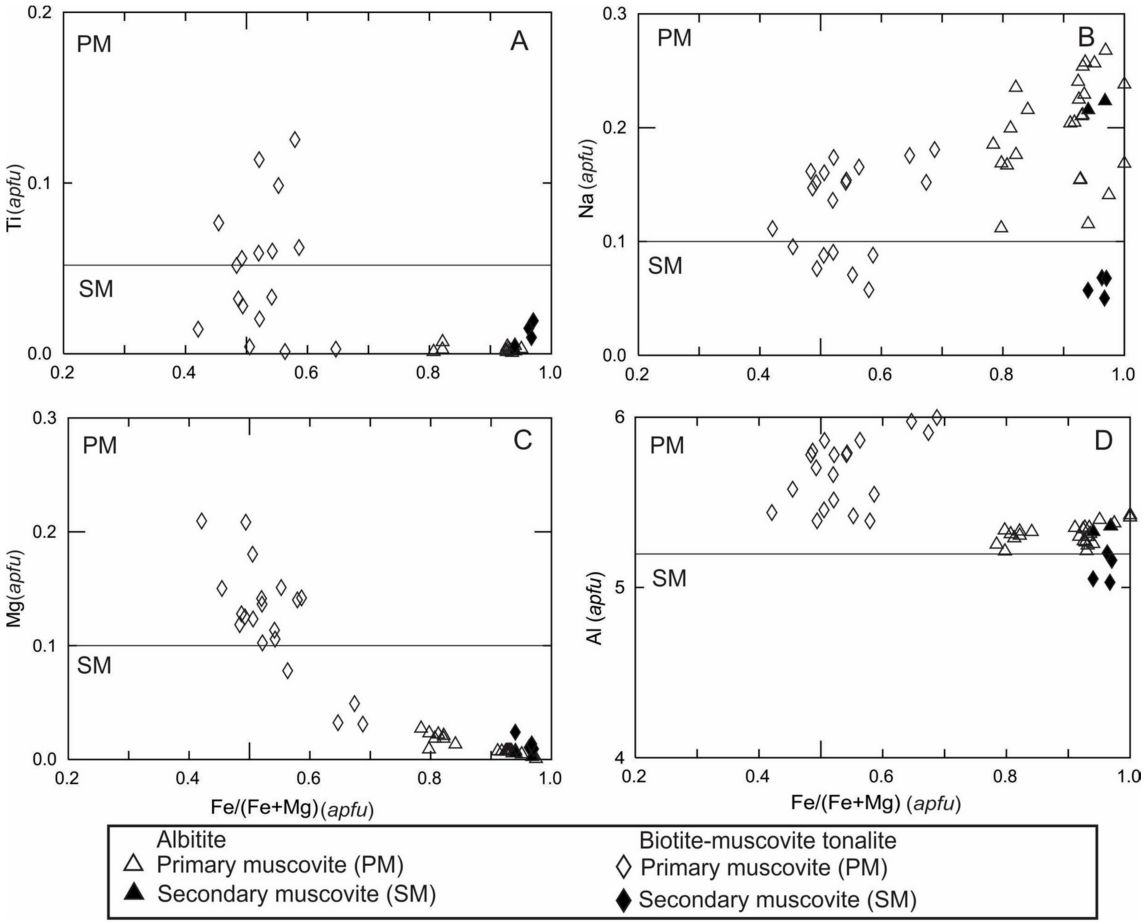

Figure 8. Geochemical discrimination diagram for the primary and secondary muscovite. (**A**) Ti vs. Fe/(Fe + Mg) diagram; (**B**) Na vs. Fe/(Fe + Mg) diagram; (**C**) Mg vs. Fe/(Fe + Mg) diagram; and (**D**) Al (t) vs. Fe/(Fe + Mg) diagram, based on Miller et al. [38]. *apfu = atoms per formula unit*.

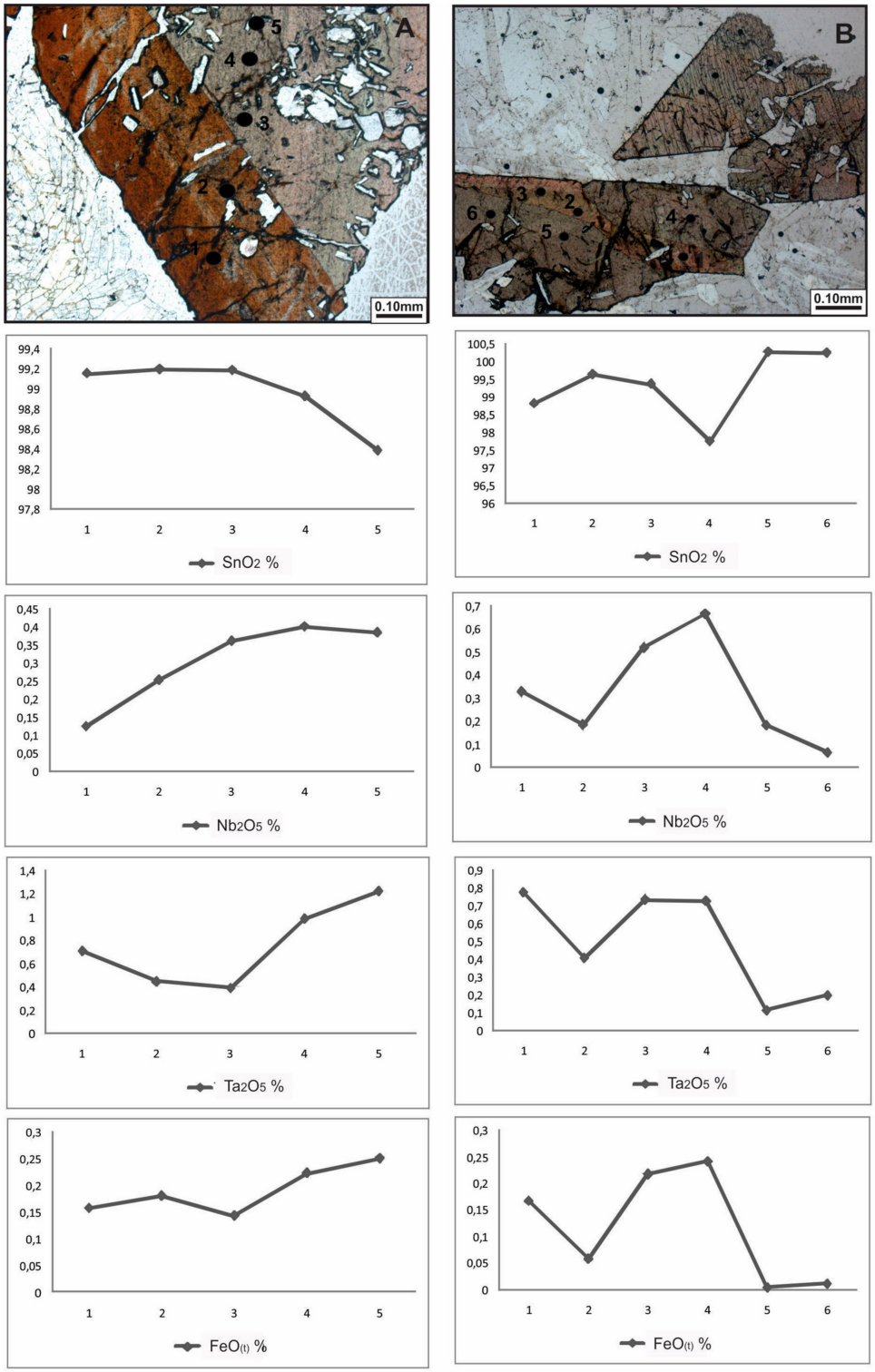

Figure 9. Compositional variation in different cassiterite crystals. (**A**) Cassiterite from albitites in Boa Vista Artisanal Mine; and (**B**) cassiterite from albitites in the Pelotas Artisanal Mine.

The compositional variation is due to the substitution of Sn for Ta, Nb and Fe in the cassiterite structure. Some possible substitution equations are [42]:

$$Sn^{4+} \leftrightarrow (Ta, Nb)^{4+}; 2Sn^{4+} \leftrightarrow (Ta, Nb)^{5+} + Fe^{3+}; \text{and } 3Sn^{4+} \leftrightarrow 2(Ta, Nb)^{5+} (Fe, Mn)^{2+} \quad (1)$$

Similar results were obtained by Costi et al. [43] in magmatic cassiterite of within-plate granites in the Pitinga Province, which has a high Nb_2O_5 (0.063 to 0.6%) and Ta_2O_5 (0.1 to 1.3%) contents. However, cassiterite from hydrothermal origin showed lower Nb_2O_5 (0.0–0.1%) and Ta_2O_5 (0.0–0.1%) contents. Higher Ta_2O_5 values in relation to Nb_2O_5 were also identified in other magmatic cassiterites from peraluminous granites of the Aurumina suite, while the opposite (Nb > Ta) occurs in hydrothermal cassiterite from within-plate granites of the Goiás Tin Province [44].

4.4. Oxygen Isotopes

Analyses of oxygen isotopes were performed in pairs of albite and cassiterite interpreted petrographically as to be in paragenesis. The obtained values were $\delta^{18}O_{VSMOW}$ = 6.7 to 9.3‰ and $\delta^{18}O_{VSMOW}$ = 5.3 to 6.6‰, respectively (Table 3).

Table 3. Oxygen isotope values ($\delta^{18}O_{VSMOW}$) of albite and cassiterite from Pelotas and Boa Vista albitite samples, and calculated isotopic equilibrium temperature and isotopic composition of fluid.

Mineral (V-SMOW)			Isotopic Equilibrium Temperature (°C) [a]	Isotopic Composition of the Fluid (‰)
Deposit	**Albite (‰)**	**Cassiterite (‰)**		
Pelotas	9.3	5.3	653 °C	9.35
Pelotas	6.7	6.6	1163–1319 °C	9.17
Boa Vista	7.7		-	9.40 [b]
Boa Vista	7.8	6.0	943 °C	9.39
Boa Vista	7.9	6.5	1016 °C	9.72

[a] Temperature calculated considering the analytical error (±0.3‰); [b] Composition estimated using the isotopic equilibrium temperature average for the Boa Vista artisanal mine.

The calculated temperature of isotopic equilibrium of the albite-cassiterite pair from albitites varied from 653 to 1319 °C. The highest temperature, however, was achieved for albite and cassiterite with relative isotopic fractionation (Δ_{xy}) of 0.1‰. Since the difference in the minerals' isotopic composition is smaller than the analytical error (0.3‰), the temperature of isotopic equilibrium estimated for this pair must be considered with caution. Considering the margin of analytical error, the temperature obtained for this pair is 1163 to 1319 °C (Table 3).

The isotopic composition of albitite fluids from the two artisanal mines is very close regardless of the difference in the temperature of isotopic equilibrium: it varies from 9.17‰ to 9.72‰ (Table 3).

Data of the isotopic fluid composition obtained for albitites are consistent with water of magmatic origin. According to Taylor Jr. [45], they show $\delta^{18}O$ between 5.5‰ and 10.0‰. Despite the wide range of values for the isotopic equilibrium temperature, the results are consistent with petrological data and with the interpretation of albitite crystallization in magmatic conditions and at high temperature.

The calculated values of the isotopic fluid composition and isotopic equilibrium temperature are different from those obtained for greisens mineralized in tin described in the region: 3.4–3.9‰ and 285–370 °C for Li-muscovite greisen, and 4.8–7.9‰ and 520–660 °C for zinnwaldite greisen and quartz-topaz rock [5].

As Kalamarides [46] stated, the plutonic rocks generally crystallize in several stages and experience changes of $\delta^{18}O$ in the subsolidus phase until they reach the isotopic closure temperature. Consequently, the isotopic equilibrium temperatures obtained for these rocks commonly lie below 800 °C. In contrast, the $\delta^{18}O$ values of volcanic rocks and their minerals tend to represent the final product of igneous processes that generated them, as crystallization occurs instantaneously. Considering the obtained data and the mode of occurrence of the studied albitites, it is reasonable to suggest elevated isotopic closure temperature and the existence of subsolidus reequilibrium.

5. Discussion

5.1. Tectonic Setting and Regional Geological Context

Field, petrographic, and chemical characteristics obtained from the studied monzogranites and tonalites are consistent with the interpretation that these are peraluminous granites, generated in a syn-collisional environment. Diagnostic primary minerals of peraluminous granites are identified in tonalites and granites, such as muscovite and garnet.

Chemical compositions of biotite from tonalite and monzogranite, where TiO_2 varies from 0.8% to 1.7%, MgO from 4.9% to 11.6%, and Al_2O_3 from 15.9% to 22.5%, are similar to biotite from peraluminous granitic suites [35,37].

In the Rb vs. (Y + Nb) and Rb vs. (Ta + Yb) diagrams elaborated by Pearce et al. [47], samples of monzogranites from the Pelotas Artisanal Mine are located near the boundary between volcanic arc granites (VAG) and syn-collisional (syn-COLG) granites. The plot of tonalite and some monzogranite samples in the field of VAG is in agreement with the interpretation of Cuadros et al. [14] that these rocks are derived from hybrid magmas (Figure 10A).

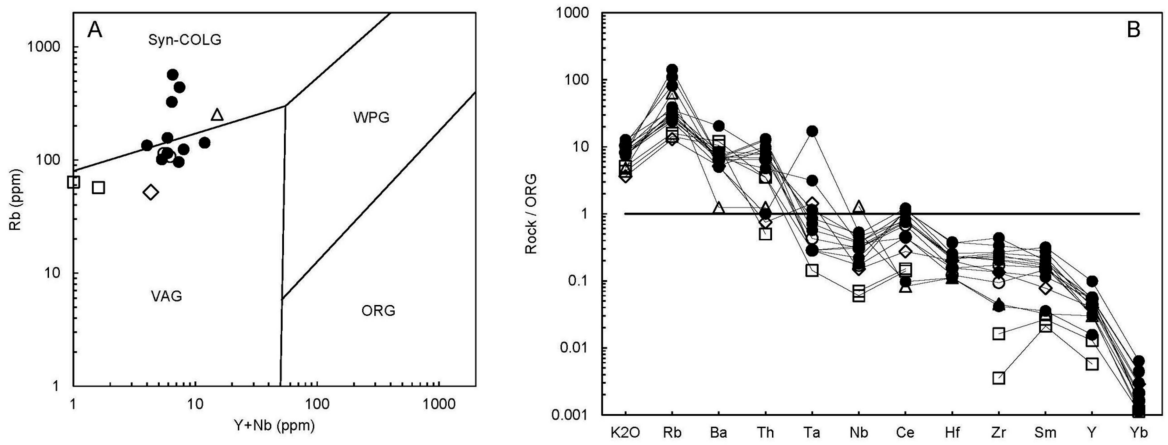

Figure 10. Tonalite, monzogranite, and albite granite samples in Pearce et al. [47] diagrams. (**A**) Rb − (Y + Nb) discriminant diagram; (**B**) ocean ridge granite (ORG) normalized geochemical patterns for representative analyses. syn-COLG: syn-collision granites; VAG: volcanic arc granites; WPG: within-plate granites. Legend as in Figure 5.

In the multi-element diagram normalized to ocean ridges granite (ORG), with values of Pearce et al. [47], positive anomalies of Rb, Th, Ce, and Sm are observed in monzogranite and albite granite samples (Figure 10B). Pearce et al. [47] attributed the enrichment of Rb and Th with respect to Nb and Ta, and Ce and Sm in regard to their adjacent elements, to crustal involvement. The pattern is described by the authors as crust-dominated. Patterns show that the studied monzogranites and albite granites are similar to those presented by Pearce et al. [47] for syn-COLG granites of Tibet.

The Sn-mineralized albitites are in contact with peraluminous granites and schists, attributed to the Aurumina granite suite and the Ticunzal Formation, respectively [12,16]. The $^{40}Ar/^{39}Ar$ age obtained for muscovite from albitite of Boa Vista Artisanal Mine (1996.55 ± 13 Ma) is interpreted as approaching the crystallization age, which suggests that the albitites were formed during the Paleoproterozoic. They probably comprise, together with tourmaline-bearing pegmatites and granites, the younger phases of the Aurumina Suite peraluminous magmatism, whose granites are considered to have crystallized between 2.12 and 2.17 Ga (zircon U-Pb) [14,22]. These Ar-Ar data are similar to the results obtained by Sparrenberger and Tassinari [17] in peraluminous pegmatites situated at about 40 km north of the studied area. According to the authors, coarse-grained muscovite from pegmatites yielded K-Ar ages of 2129 ± 26 Ma and 2006 ± 24 Ma. After the albitites' formation, the $^{40}Ar/^{39}Ar$ data

registered an event at 1901.2 ± 30 Ma, which caused the release of 47% of ^{39}Ar. It is suggested that this release of ^{39}Ar could be related to the first crust perturbations due to the continental rifting experienced by the region in the Paleoproterozoic. In this geotectonic setting, the intrusion of within-plate granites occurred about 1.8 Ga [48,49]. Another heating event was recorded at 618.0 ± 36.2 Ma by ^{40}Ar/^{39}Ar data, interpreted as related to the Brasiliano tectono-metamorphic event (Pan-African) described in the region and registered as incipient deformation in the studied rocks.

5.2. Genesis and Evolution of Albitites and Associated Granitic Rocks

Albitites in the Pelotas and the Boa Vista artisanal mines have textures interpreted as magmatic, such as snowball texture in quartz, apatite and cassiterite. Albite inclusions have crystallized during its host mineral growth. Albite also has flow texture, with alignment of equigranular albite laths in the matrix (Figure 3). Field relationships suggest that, at least in the Pelotas Artisanal Mine, the studied albitite occurs as dikes or lenses 1 to 2.5 m thick. They occur in sharp contact with peraluminous monzogranites and tonalites, assigned to the peraluminous Aurumina Granitic Suite (2.15–2.0 Ga) by Botelho et al. [16], and with schists of the Ticunzal Formation, which was intruded by the Aurumina Suite. Magmatic albitite, regarded as the end stage of magmatic crystallization, has also been reported in other regions of the world [7,8,50].

The obtained data allow interpretation of the snowball texture in the studied rocks following the authors who consider those textural relationships as a characteristic of evolved granites that crystallized from a residual melt. These granites occur in the apical part of subvolcanic granite complexes and are commonly associated with rare-metal mineralization [51].

The oxygen isotope data showed that the isotopic fluid composition in equilibrium with albitite, from 8.68 to 9.72, is consistent with magmatic signature without influence of meteoric water. This reinforces the interpretation of magmatic origin for the Sn-mineralized albitite of the two studied areas. The estimated albitite isotopic equilibrium temperatures are also consistent with direct crystallization from highly specialized magma rich in Na_2O, P, and B, and depleted in fluorine, with subsolidus reequilibrium.

The studied albitites are probably related to tourmaline-albite granites and tourmaline pegmatites recently described by Cuadros et al. [14] in the region and considered as the most evolved rocks of the Aurumina Suite. In the Boa Vista and Pelotas area we find only tourmaline-bearing pegmatites and tourmaline-free albite granites. We interpret the albitite as primary in origin. One possibility is its formation by the accumulation of albite crystals, which separated from an evolved granitic liquid that gave rise to the tourmaline-albite granite and associated pegmatitic facies. The albite granite would represent a residual liquid. The albitite is similar to the Sn-Ta-bearing albitite described in Slovakia by Breiter et al. [52]. However, at least considering the actual level of investigation in the area, a granite cupola does not occur. The albitite and pegmatite occur as isolated bodies into the granite-tonalite terrain. The albitite is composed of more than 90% albite instead of the compositional variation in Slovakia. The observed flow textures and the pockets of massive albite allow suggest an accumulation of albite laths by separation of the liquid. These interpretations are reinforced by the oxygen isotope data and the flow textures described above.

5.3. Tin Transport and Concentration

Crystallization and economic concentration of cassiterite have been reported as a product of direct crystallization from evolved granitic magma or, more commonly, as the result of hydrothermal alteration. In the latter case, tin was leached from granite and/or country rocks and crystallized as cassiterite.

Cassiterite in the studied artisanal mines is interpreted as having been formed by crystallization from an evolved tin-rich granitic magma. When cassiterite occurs as a magmatic mineral, tin must be incompatible with the whole history of melt crystallization. According to Linnen [53], tin must be partitioned into silicate liquid, or the vapor fraction should be sufficiently low so that the tin

concentration in the liquid will continue to increase with fractionation. Magmatic cassiterite can be crystallized in highly evolved systems because, in granitic intrusions with low chlorine content, tin is partitioned into the granitic melt [53]. The results of Linnen et al. [54] and Bhalla et al. [55] showed that Al plays an important role in tin solubility in evolved granitic magmas. SnO_2 solubility in peraluminous magmas will also depend on oxygen fugacity and temperature. Oxygen fugacity increase and temperature decrease tend to reduce tin solubility [31,54–56]. Linnen et al. [55] uses the strong oxygen fugacity dependence of tin solubilities to explain the existence of some magmatic tin deposits. The presence of volatiles in magma is also an important factor in Sn concentration: B, F, Cl, and P contents are generally concentrated in the final stages of evolved magmas and contribute to tin solubility [55,57,58].

The studied granitic rocks have features typical of LCT [59], peraluminous and syn-orogenic systems. Albitites have primary apatite due to high contents of phosphorous. The less-evolved system in the region contains high boron, expressed as magmatic tourmaline. Granitic rocks do not possess cassiterite on their mineral assemblages and have low Sn, Ta, and Nb contents (Table 1). The existing data suggested that tin remained in solution in the peraluminous granitic magma until it precipitated in albitites. Probably, Sn transport occurred in low oxygen fugacity conditions, in P-rich peraluminous magma. Tantalum and niobium precipitation occurred along with Sn and tantalite was recovered together with cassiterite in some artisanal mines

6. Conclusions

The main conclusions of this research are:

1. The studied albitites have a snowball texture in quartz, apatite, and cassiterite and flow texture, with alignment of albite laths in the matrix, interpreted as magmatic texture. These rocks are interpreted as magmatic and occur as dikes or lenses in monzogranite, peraluminous tonalite, and graphite schist.
2. Albitites have high Na_2O, Al_2O_3, P_2O_5, Sn, Ta, and Nb (Ta > Nb) contents and represent cumulates separated from evolved Na-rich peraluminous magmas related to the Aurumina suite tourmaline-bearing rocks. The albite granite represents a residual liquid from the late stages of magmatism.
3. Biotite from monzogranite and tonalite have compositions similar to those from peraluminous granitic suites. Tin in cassiterite is replaced by Fe, Ta, and Nb, with Ta > Nb contents. The chemical composition of the studied rocks acted as a control factor on the composition of primary muscovite, especially in Na_2O and TiO_2 contents. Primary muscovite from tonalite has higher Al, Mg, and Na, and lower Fe and Si contents than secondary ones. While secondary muscovite always has low TiO_2 (0.0–0.07%) contents, magmatic muscovite of tonalite has variable Ti contents. Both primary and secondary muscovite from albitites and albite granites have virtually no Ti and are high in Na, Al, and Si.
4. The isotopic fluid composition in equilibrium with albitites varies from 8.68‰ to 9.72‰ and is consistent with the interpretation of magmatic origin. Although the calculated isotopic equilibrium temperatures are elevated for the evolved peraluminous granite system in place, they also demonstrate the absence of hydrothermal influence on albitite crystallization.
5. $^{40}Ar/^{39}Ar$ data in muscovite suggest that albitites crystallized around 1996 ± 13 Ma and they can be correlated to the final stages of the Aurumina Suite (2.12–2.17 Ga). Argon loss in 618.0 ± 36.2 Ma is interpreted as related to the Brasiliano (Pan-African) tectono-metamorphic event.
6. In addition to containing hydrothermal tin mineralization hosted in greisens and within-plate granite magmatism, of approximately 1.7 Ga, the Goiás Tin Province has magmatic tin economic concentrations hosted in igneous albitite of about 2.0 Ga. These results, therefore, extend the possibilities of a tin source in the Goiás Tin Province. They have implications for the province's

economic potential and also help understand solubility and tin concentration in peraluminous granitic systems highly evolved and very rich in sodium.

Author Contributions: M.A.M. and N.F.B. conceived and coordinated the research; A.R.F.S. and M.A.M. took part to the field campaigns; A.R.F.S. prepared and analyzed the samples and the data; T.K.K. was responsible for the isotopic data analyses; and A.R.F.S., M.A.M. and N.F.B. took part in the discussion and wrote the paper.

Funding: This study was financially supported by CNPq (Brazilian National Council for Scientific and Technological Development) (process no. 133302/2012-1) and CAPES (Coordenação de Aperfeiçoamento de Pessoal de Nível Superior) (scholarship for the first author).

Acknowledgments: The authors would like to thank CNPq (Brazilian National Council for Scientific and Technological Development) for financial support. Verena Mineração Ltd. is thanked for giving permission for this study and for providing access to drill holes and technical information. We sincerely thank Valmir da Silva Souza (University of Brasilia) for providing the 40Ar/39Ar data. We also thank University of Brasilia and Queen's geological laboratories used in this research.

Conflicts of Interest: The authors declare no conflict of interest

References

1. Charoy, B.; Pollard, P.J. Albite-rich, silica-depleted metasomatic rocks at Emuford, Northeast Queensland: Mineralogical, geochemical and fluid inclusion constraints on hydrothermal evolution and tin mineralization. *Econ. Geol.* **1989**, *84*, 1850–1874. [CrossRef]
2. Castorina, F.; Masi, U.; Padalino, G.; Palomba, M. Constraints from geochemistry and Sr–Nd isotopes for the origin of albitite deposits from central Sardinia (Italy). *Miner. Depos.* **2006**, *41*, 323–338. [CrossRef]
3. Mohammad, Y.O.; Maekawa, H.; Lawa, F.A. Mineralogy and origin of Mlakawaalbitite from Kurdistan region, Northeastern Iraq. *Geosphere* **2007**, *3*, 624–645. [CrossRef]
4. Kovalenko, V.I. The genesis of rare metal granitoids and related ore deposits. In *Metallization Associated with Acid Magmatism Czech Geological Survey*; Stemprok, M., Burnol, L., Tischendorf, G., Eds.; Geological Survey: Prague, Czech Republic, 1978; Volume 3, pp. 235–247.
5. Moura, M.A.; Botelho, N.F.; Olivo, G.R.; Kyser, K.; Pontes, R.M. Genesis of the Proterozoic Mangabeira tin–indium mineralization, central Brazil: Evidence from geology, petrology, fluid inclusion and stable isotope data. *Ore Geol. Rev.* **2014**, *60*, 36–49. [CrossRef]
6. Cuney, M.; Marignac, C.; Weisbrod, A. The Beauvoir topaz-lepidolite albite granite (Massif Central, France); the disseminated magmatic Sn-Li-Ta-Nb-Be mineralization. *Econ. Geol.* **1992**, *87*, 1766–1794. [CrossRef]
7. Schwartz, M.O. Geochemical criteria for distinguishing magmatic and metasomatic albite-enrichment in granitoids: Examples from the Ta–Li granite Yichun (China) and the Sn–W deposit Tikus (Indonesia). *Miner. Depos.* **1992**, *27*, 101–108. [CrossRef]
8. Costi, H.T.; Dall'Agnol, R.; Pichavant, M.; Rämö, O.T. The peralkaline tin-mineralized Madeira cryolite albite-rich granite of Pitinga, Amazonian craton, Brazil: Petrography, mineralogy and crystallization processes. *Can. Miner.* **2009**, *47*, 1301–1327. [CrossRef]
9. Wang, G.; Wang, Z.; Zhang, Y.; Wang, K. Zircon geochronology and trace element geochemistry from the Xiaozhen Copper Deposit, North Daba Mountain: Constraints on albitites petrogenesis. *Acta Geol. Sin. Engl.* **2014**, *88*, 113–127. [CrossRef]
10. Lenharo, S.L.R.; Moura, M.A.; Botelho, N.F. Petrogenetic and mineralization processes in Paleo-to Mesoproterozoic rapakivi granites: Example from Pitinga and Goiás, Brazil. *Precambr. Res.* **2002**, *119*, 277–299. [CrossRef]
11. Lenharo, S.L.R.; Pollard, P.J.; Born, H. Petrology and textural evolution of granites associated with tin and rare-metals mineralization at the Pitinga mine, Amazonas, Brazil. *Lithos* **2003**, *66*, 37–61. [CrossRef]
12. Marini, O.J.; Botelho, N.F. A Província de Granitos Estaníferos de Goiás. *Rev. Bras. Geociênc.* **1986**, *16*, 119–131.
13. Cuadros, F.; Botelho, N.F.; Fuck, R.A.; Dantas, E.L. The Ticunzal Formation in central Brazil: Record of Rhyacian sedimentation and metamorphism in the western border of the São Francisco Craton. *J. S. Am. Earth Sci.* **2017**, *79*, 307–325. [CrossRef]

14. Cuadros, F.; Botelho, N.F.; Fuck, R.A.; Dantas, E.L. The peraluminous Aurumina Granite Suite in central Brazil: An example of mantle-continental crust interaction in a Paleoproterozoic cordilleran hinterland setting? *Precambr. Res.* **2017**, *299*, 75–100. [CrossRef]
15. Alvarenga, C.J.S.; Botelho, N.F.; Dardenne, M.A.; Lima, O.N.B.; Machado, M.A. *Monte Alegre de Goiás—SD.23-V-C-III, Escala 1:100,000: Nota Explicativa Integrada com Nova Roma e Cavalcante*; CPRM: Brasília/Goiás, Brazil, 2007; 67p.
16. Botelho, N.F.; Alvarenga, C.J.S.; Menezes, P.R.; D'El Rey Silva, L.J.H. Suíte Aurumina: Uma suíte de granitos paleoproterozóicos, peraluminosos e sin-tectônicos na Faixa Brasília. In Proceedings of the 7th Simpósio de Geologia do Centro-Oeste, Brasília, Brasil, 14–19 November 1999; p. 17.
17. Sparrenberger, I.; Tassinari, C.C.G. Subprovíncia do Rio Paranã (GO): Um exemplo de aplicação dos métodos de datação U-Pb e Pb-Pb em cassiterita. *Rev. Bras. Geociênc.* **1999**, *29*, 405–414. [CrossRef]
18. Pimentel, M.M.; Fuck, R.A.; Botelho, N.F. Granites and the geodynamic evolution of the Neoproterozoic Brasilia belt, central Brazil. *Lithos* **1999**, *46*, 463–483. [CrossRef]
19. Dardenne, M.A. The Brasília fold belt. In Proceedings of the 31st International Geological Congress, Rio de Janeiro, Brazil, 6–17 August 2000; pp. 231–236.
20. Marini, O.J. Nova unidade litostratigráfica do Pré-Cambriano do estado de Goiás. In Proceedings of the 30th Congresso Brasileiro de Geologia, Recife, Brazil, November 1978; pp. 126–127.
21. Pimentel, M.M.; Jost, H.; Fuck, R.A. O embasamento da Faixa Brasília e o Arco Magmático de Goiás. In *Geologia do Continente sul Americano: Evolução da Obra de Fernando Flávio Marques de Almeida*; Mantesso-Neto, V., Bartorelli, A., Carneiro, C.D.R., Brito-Neves, B.B., Eds.; Beca: São Paulo, Brazil, 2004; pp. 356–368.
22. Botelho, N.F.; Fuck, R.A.; Dantas, E.L.; Laux, J.H.; Junges, S.L. The Paleoproterozoic peraluminous Aurumina Granite Suite, Goiás and Tocantins, Brazil: Geological, whole rock geochemistry and U-Pb and Sm-Nd isotopic constraints. In *The Paleoproterozoic Record of the São Francisco Craton, Proceedings of the IGCP 509 Annual Meeting, Bahia/Minas Gerais, Brazil, 9–21 September 2006*; p. 92. Available online: https://earth.yale.edu/sites/default/files/files/IGCP/IGCP%20Brazil.pdf (accessed on 3 August 2018).
23. Instituto de Geociências/UnB. Mapa Geológico do Projeto Nova Roma—Porto Real. Bachelor's Thesis, University of Brasilia, Brasília, Brazil, 2005.
24. Roddick, J.C. High precision intercalibration of $^{40}Ar/^{39}Ar$ standards. *Geochim. Cosmochim. Acta* **1983**, *47*, 887–898. [CrossRef]
25. Steiger, R.H.; Jäger, E. Subcommission on geochronology: Convention on the use of decay constants in geo- and cosmo-chronology. *Earth Planet. Sci. Lett.* **1977**, *36*, 359–362. [CrossRef]
26. Dalrymple, G.B.; Alexander, E.C., Jr.; Lanphere, M.A.; Kraker, G.P. *Irradiation of Samples for $^{40}Ar/^{39}Ar$ Dating Using the Geological Survey TRIGA Reactor*; U.S. Geological Survey Professional Paper 1176; U.S. Government Printing Office: Washington, DC, USA, 1981; p. 1176.
27. Clayton, R.N.; Mayeda, T.K. The use of bromine pentafluoride in the extraction of oxygen from oxides and silicates for isotopic analysis. *Geochim. Cosmochim. Acta* **1963**, *27*, 43–52. [CrossRef]
28. Zheng, Y.F. Calculation of oxygen isotope fractionation in metal oxides. *Geochim. Cosmochim. Acta* **1991**, *55*, 2299–2307.
29. Bottinga, Y.; Javoy, M. Comments on oxygen isotope geothermometry. *Earth Planet. Sci. Lett.* **1973**, *20*, 250–265. [CrossRef]
30. Streckeisen, A. To each plutonic rocks its proper name. *Earth Sci. Rev.* **1976**, *12*, 1–33. [CrossRef]
31. Schwartz, M.O.; Rajah, S.S.; Askury, A.K.; Putthapiban, P.; Djaswadi, S. The Southeast Asian Tin Belt. *Earth Sci. Rev.* **1995**, *38*, 95–293. [CrossRef]
32. Corsini, M.; Figueiredo, L.L.; Caby, R.; Feraud, G.; Ruffet, G.; Vauchez, A. Thermal history of the Pan-African/Brasiliano Borborema Province of northeast Brazil deduced from $^{40}Ar/^{39}Ar$ analysis. *Tectonophysics* **1997**, *285*, 103–117. [CrossRef]
33. Maniar, P.D.; Piccoli, P.M. Tectonic discrimination of granitoids. *Geol. Soc. Am. Bull.* **1989**, *101*, 635–643. [CrossRef]
34. Nakamura, N. Determination of REE, Ba, Fe, Mg, Na and K in carbonaceous and ordinary chondrites. *Geochim. Cosmochim. Acta* **1974**, *38*, 757–775. [CrossRef]

35. Nachit, H.; Ibhi, A.; Abia, E.H.; Ohoud, M.B. Discrimination between primary magmatic biotites, reequilibrated biotites and neoformed biotites. *C. R. Geosci.* **2005**, *337*, 1415–1420. [CrossRef]
36. Deer, W.A.; Howie, R.A.; Zussman, J. *Rock Forming Minerals: Sheet Silicates*; Longman Green and Co.: London, UK, 1963.
37. Abdel-Rahman, A.M. Nature of biotites from alkaline, calc-alkaline, and peraluminous magmas. *J. Petrol.* **1994**, *35*, 525–541. [CrossRef]
38. Miller, C.F.; Stoddard, E.F.; Bradfish, L.J. Composition of plutonic muscovite: Genetic implications. *Can. Miner.* **1981**, *19*, 25–34.
39. Koh, J.S.; Yun, S.H. The compositions of biotite and muscovite in the Yuksipryong two-mica granite and its petrological meaning. *Geosci. J.* **1999**, *3*, 77–86. [CrossRef]
40. Zane, A.; Rizzo, G. The compositional space of muscovite in granitic rocks. *Can. Mineral.* **1999**, *37*, 1229–1238.
41. Tao, J.; Li, W.; Cai, Y.; Cen, T. Mineralogical feature and geological significance of muscovites from the Longyuanba Indosinian and Yanshannian two-mica granites in the eastern Nanling Range. *Sci. China Ser. D* **2014**, *57*, 1150–1157. [CrossRef]
42. Möller, P.; Dulski, P.; Szacki, W.; Malow, G.; Riedel, E. Substitution of tin in cassiterite by tantalum, niobium, tungsten, iron and manganese. *Geochim. Cosmochim. Acta* **1988**, *52*, 1497–1503. [CrossRef]
43. Costi, H.T.; Horbe, A.M.C.; Borges, R.M.K.; Dall'agnol, R.; Rossi, O.R.R.; Sighnolfi, G.P. Mineral chemistry of cassiterites from Pitinga Province, Amazonian Craton, Brazil. *Rev. Bras. Geociênc.* **2000**, *30*, 775–782. [CrossRef]
44. Pereira, A.B. Caracterização dos Granitos e Pegmatitos Peraluminosos, Mineralizados em Sn-Ta, de Monte Alegre de Goiás. Master's Thesis, Instituto de Geociências, Universidade de Brasília, Brasília, Brazil, 2002.
45. Taylor, H.P., Jr. The application of oxygen and hydrogen isotope studies to problems of hydrothermal alteration and ore deposition. *Econ. Geol.* **1974**, *69*, 843–883. [CrossRef]
46. Kalamarides, R.I. High-temperature oxygen isotope fractionation among the phases of the Kiglapait Intrusion, Labrador, Canada. *Chem. Geol.* **1986**, *58*, 303–310. [CrossRef]
47. Pearce, J.A.; Harris, N.W.; Tindle, A.G. Trace element discrimination diagrams for the tectonic interpretation of granitic rocks. *J. Petrol.* **1984**, *25*, 956–983. [CrossRef]
48. Pimentel, M.M.; Heaman, L.; Fuck, R.A.; Marini, O.J. U/Pb zircon geochronology of Precambrian tin-bearing continental type acid magmatism in central Brazil. *Preccambr. Res.* **1991**, *52*, 321–335. [CrossRef]
49. Pimentel, M.M.; Botelho, N.F. Sr and Nd isotopic characteristics of 1.77–71.58 Ga rift-related granites and volcanics of the Goiás Tin Province, central Brazil. *Anais Acad. Bras. Ciênc.* **2001**, *73*, 263–276. [CrossRef]
50. London, D. Magmatic-hydrothermal transition in the Tanco rare-element pegmatite: Evidence from fluid inclusions and phase-equilibrium experiments. *Am. Miner.* **1986**, *71*, 376–395.
51. Müller, A.; van den Kerkhof, A.M.; Behr, H.-J.; Kronz, A.; Koch-Müller, M. The evolution of late-Hercynian granites and rhyolites documented by quartz—A review. *Earth Environ. Sci. Trans. R. Soc. Edinb.* **2009**, *100*, 185–204. [CrossRef]
52. Breiter, K.; Broska, I.; Uher, P. Intensive low-temperature tectono-hydrothermal overprint of peraluminous rare-metal granite: A case study from the Dlhá dolina valley (Gemericum, Slovakia). *Geol. Carpath.* **2015**, *66*, 19–36. [CrossRef]
53. Linnen, R.L. Depth of emplacement, fluid provenance and metallogeny in granitic terranes: A comparison of western Thailand with other tin belts. *Miner. Depos.* **1998**, *33*, 461–476. [CrossRef]
54. Linnen, R.L.; Pichavant, M.; Holtz, F. The combined effects of fO_2 and melt composition on SnO_2 solubility and tin diffusivity in haplogranitic melts. *Geochim. Cosmoch. Acta* **1996**, *60*, 4965–4976. [CrossRef]
55. Bhalla, P.; Holtza, F.; Linnen, R.L.; Behrens, H. Solubility of cassiterite in evolved granitic melts: Effect of T, fO_2, and additional volatiles. *Lithos* **2005**, *80*, 387–400. [CrossRef]
56. Linnen, R.L.; Pichavant, M.; Holtz, F.; Burgess, S. The effect of fO_2 on the solubility, diffusion, and speciation of tin in haplogranitic melt at 850 °C and 2 kbar. *Geochim. Cosmoch. Acta* **1995**, *59*, 1579–1588. [CrossRef]
57. Bea, F.; Fershlater, G.; Corretgé, L.G. The geochemistry of phosphorus in granite rocks and the effect of aluminium. *Lithos* **1992**, *29*, 43–56. [CrossRef]

58. Thomas, R.; Förster, H.-J.; Heinrich, W. The behaviour of boron in a peraluminous granite-pegmatite system and associated hydrothermal solutions: A melt and fluid-inclusion study. *Contrib. Mineral. Petrol.* **2003**, *144*, 457–472. [CrossRef]
59. Černý, P. Fertile granites of Precambrian rare-element pegmatite fields: Is geochemistry controlled by tectonic setting or source lithologies. *Precambr. Res.* **1991**, *51*, 429–468. [CrossRef]